www.neurosci.cn
www.springer.com/12264

ORIGINAL ARTICLE

Polysaccharide Krestin Prevents Alzheimer's Disease-type Pathology and Cognitive Deficits by Enhancing Monocyte Amyloid-β Processing

Si-Han Chen[1,2,3,6] · Chen-Yang He[1,2,3] · Ying-Ying Shen[1,2,3] · Gui-Hua Zeng[1,2,3] ·
Ding-Yuan Tian[1,2,3] · Yuan Cheng[1,2,3] · Man-Yu Xu[1,2,3] · Dong-Yu Fan[1,2,3] ·
Cheng-Rong Tan[1,2,3] · An-Yu Shi[1,2,3] · Xian-Le Bu[1,2,3,4] · Yan-Jiang Wang[1,2,3,4,5]

Abstract Deficits in the clearance of amyloid β protein (Aβ) by the peripheral system play a critical role in the pathogenesis of sporadic Alzheimer's disease (AD). Impaired uptake of Aβ by dysfunctional monocytes is deemed to be one of the major mechanisms underlying deficient peripheral Aβ clearance in AD. In the current study, flow cytometry and biochemical and behavioral techniques were applied to investigate the effects of polysaccharide krestin (PSK) on AD-related pathology in vitro and in vivo. We found that PSK, widely used in therapy for various cancers, has the potential to enhance Aβ uptake and intracellular processing by human monocytes in vitro. After administration of PSK by intraperitoneal injection, APP/PS1 mice performed better in behavioral tests, along with reduced Aβ deposition, neuroinflammation, neuronal loss, and tau hyperphosphorylation. These results suggest that PSK holds promise as a preventive agent for AD by strengthening the Aβ clearance by blood monocytes and alleviating AD-like pathology.

Keywords Alzheimer's disease · Aβ uptake · Polysaccharide krestin · Monocyte

Si-Han Chen and Chen-Yang He have contributed equally to this work.

✉ Xian-Le Bu
  buxianle@sina.cn

✉ Yan-Jiang Wang
  yanjiang_wang@tmmu.edu.cn

1 Department of Neurology and Centre for Clinical Neuroscience, Daping Hospital, Third Military Medical University, Chongqing 400042, China

2 The Institute of Brain and Intelligence, Third Military Medical University, Chongqing 400042, China

3 Chongqing Key Laboratory of Ageing and Brain Diseases, Chongqing 400042, China

4 State Key Laboratory of Trauma, Burn and Combined Injury, Daping Hospital, Third Military Medical University, Chongqing 400042, China

5 Center for Excellence in Brain Science and Intelligence Technology, Chinese Academy of Sciences, Shanghai 201200, China

6 Department of Neurology, Nanchong Central Hospital, The Second Clinical Medical School, North Sichuan Medical College, Nanchong 637000, China

Introduction

Alzheimer's disease (AD) is the most common neurodegenerative disorder affecting 35 million elderly individuals [1]. The growing prevalence of AD with aging has imposed enormous social and economic burdens on society [2]. Until now, its mechanism has remained unclear, and no effective therapy is available. Widespread evidence suggests that a deficit in the clearance of amyloid β-protein (Aβ), leading to the cerebral accumulation of Aβ, plays an essential role in the development of sporadic AD [3].

Diverse mechanisms are involved in the clearance of Aβ from the brain and periphery *in vivo*. While resident microglia plays an important role in the clearance of Aβ in the brain, ∼40%–60% of the Aβ generated in the brain is estimated to diffuse into the blood and be cleared in the periphery, implying that the peripheral system also plays a crucial role in clearing Aβ from the brain [4–6]. With regard to how this brain-derived Aβ is cleared in the

periphery, its uptake by monocytes and macrophages is deemed to be one of the major mechanisms of peripheral Aβ clearance in AD mouse models [7–9]. As the counterpart of brain microglia in the periphery, monocytes have been demonstrated to be more effective in neuroprotection, the regulation of neuroinflammation, and Aβ clearance than microglia in AD [10, 11]. The blood-derived monocyte not only promotes removal of brain and peripheral Aβ, but also behaves as a house-keeper within the vasculature by eliminating Aβ micro-aggregates from the brain microvasculature into the blood circulation. Nonetheless, our and other groups found that the uptake and degradation of Aβ by monocytes is decreased in AD [12, 13]. Recovery of the Aβ uptake function of blood monocytes may be a potential therapeutic strategy for AD.

Our previous study has demonstrated that the expression of Toll-like receptor 2 (TLR2), a natural innate immune receptor for Aβ recognition and uptake through the formation of a receptor complex with CD14 [14–16], is decreased in AD. Hence, activation of TLR2 may restore Aβ uptake by monocytes in AD. Previous studies have found that polysaccharide krestin (PSK), an extract of *Trametes versicolor*, is capable of stimulating the innate immune pathway [17, 18]. Furthermore, PSK, a treatment currently used to treat multiple types of cancer, is also a novel TLR2 agonist, and thus may facilitate the uptake of Aβ by monocytes through the activation of TLR2 [19–21].

The current study aimed to determine whether PSK can directly stimulate Aβ uptake and metabolism by blood monocytes and alleviate AD-related pathology in AD mouse models.

Materials and Methods

Study Participants

A total of 20 cognitively normal participants aged 50 to 70 years were recruited from Daping Hospital between January 2021 and May 2021. The participants were not eligible if they had a neurologic disorder; were in a state of obvious infection or inflammation potentially affecting the status of blood cells; had severe cardiac, pulmonary, hepatic, renal diseases, or any kind of tumor; had any potent hematopathy, including acute monocytic leukemia and myelodysplastic syndrome, during the recovery period of agranulocytosis; had autoimmune diseases, including rheumatoid arthritis and systemic lupus erythematosus; had an endocrine system disease, including Cushing syndrome and thyroid disorders; or declined to participate in the study.

The study was approved by the Ethics Committee of Daping Hospital. Written consent was obtained from participants or their legal representatives.

Blood Sampling

Fasting blood was sampled between 08:00 and 09:00 to avoid possible circadian rhythm effects. To avoid the possible effects of drugs on indices of routine blood tests, fasting blood was sampled within 2 h after admission to hospital. A portion of fasting blood samples was aliquoted for measuring complete blood cell counts, fasting glucose, thyroxin, creatinine, urea, uric acid, aspartate aminotransferase, alanine aminotransferase, and total cholesterol levels. From another portion of the sample, plasma was separated within 30 min after sampling and stored at −80 °C until further use. For Aβ uptake-related pathway assays, peripheral blood mononuclear cells (PBMCs) were isolated within 2 h after drawing blood.

Isolation of PBMCs and Monocytes

Fresh ethylene diamine tetraacetic acid-anticoagulated blood was diluted with PBS (1:1; vol/vol). Human or mouse PBMCs were isolated by density gradient centrifugation using Ficoll-Hypaque or a mouse lymphocyte separation fluid kit (TBD Science, China, LTS1077), and mononuclear sections were collected and washed three times with PBS. To isolate human monocytes, PBMCs were further screened for monocytes using CD14 Microbeads (Miltenyi Biotec, Germany, 130050201) and passed through a magnetic-activated cell-sorting column for the positive selection of $CD14^+$ cells, according to the manufacturer's instructions. The remaining PBMCs were frozen at $1–2 \times 10^6$ cells/mL in 10% DMSO (Sigma-Aldrich, Saint Louis, USA)/90% fetal calf serum (vol/vol; Gibco, California, USA) for future use.

Aβ Uptake Assay

Isolated human or mouse PBMCs were re-suspended in RPMI medium with 10% fetal calf serum and 1% penicillin/streptomycin and adjusted to 2×10^6 or 2×10^5 cells/mL. Human PBMCs were incubated with PSK (0–200 μg/mL; Qixing, China, Z44022418) for 48 h. To determine whether the functional change of monocytes was mediated by TLR2, purified mouse anti-human TLR2 (BD, USA, 558317) was added to the medium 1 h prior to addition of PSK. To test the uptake of Aβ, human or mouse PBMCs were incubated with FITC-Aβ$_{42}$ (2 μg/mL or 200 ng/mL; GL Biochem, China, 724354) for 1 h at 37°C in a 5% CO_2 incubator. Following incubation, the cell suspensions were discarded, and adherent cells were detached from the well

292

Neurosci. Bull. March, 2022, 38(3):290–302

plate by 0.25% trypsin and washed twice with fluorescence-activated cell sorting (FACS) buffer.

Flow Cytometry

Human or mouse PBMCs were pre-incubated with Human TruStain FcX (Biolegend, USA, 422302) or anti-mouse CD16/CD32 (Biosciences, USA, 553141) on ice for 20 min to avoid a high background. Then, the cell suspensions were washed and stained with fluorophore-labelled antibodies according to the corresponding manufacturer's instructions. For human PBMC staining, APC-anti human CD14 (BD, USA, 561708) or the appropriate IgG isotype were used. To detect $A\beta$ uptake-related receptors, including TLR2, TREM2 (triggering receptor expressed on myeloid cells 2), CD36, and macrophage scavenger receptor 1, were stained with monoclonal antibodies against BB515-anti-human CD282, Percp-CyTM5.5-anti-human CD36, BV421-anti-human MSR1, and PE-anti-human TREM2 (BD, USA, 565597, 561536, 0346182, 237920). For staining of mouse monocytes, PE-anti-mouse CD115 (BD, USA, 525649), FITC-anti-mouse CD11b (BD, USA, 587396), PerCP-anti-mouse CD45 (BD, USA, 557235), APC-anti-mouse Ly-6C (BD, USA, 560595), and BV421-anti-mouse TLR2 (BD, USA, 565908) were used. Cells were stained on ice for 15 min, washed twice by centrifugation, and fixed with 1% paraformaldehyde. Cells were acquired on a NovoCyte Flow Cytometer (ACEA Biosciences, CA, USA) or a FACS Navios (Beckman, CA, USA) after appropriate compensation, and analyses were performed using NovoExpress or FlowJo v10 software.

Imaging Flow Cytometry

Imaging flow cytometry was performed as in a previous report [11] on a two-camera ISX with INSPIRE acquisition software (Amnis, NJ, USA). A 2.5 mW 785 nm laser was used for internal calibration to provide a scatter signal and measure SpeedBeads . FITC and PE were excited by the 488 nm laser, and the emission was captured in the ranges 505–560 nm (Ch02) and 560–595 nm (Ch03), respectively. In total, 25,000 events were acquired, and all images were captured with a 20× objective and a cell classifier (threshold) applied to the bright field channel (Ch01) to exclude small particles. Cells with high-intensity labelling of the PE-anti mouse CD115 marker were identified as monocytes. FITC-$A\beta_{42}$ positive monocytes were identified using Amnis IDEAS software.

Confocal Microscopy

Human monocytes were enriched by plastic adhesion overnight and seeded onto a collagen-coated MatTek culture dish with a 10 μm cover slide on the bottom. After different treatments, monocytes were incubated with FITC-$A\beta_{42}$ (2 μg/mL) for 1 h or overnight at 37°C in a 5% CO_2 incubator, washed three times with PBS, and fixed with 4% paraformaldehyde. To stain intracellular proteins, cells were permeabilized with 0.1% Triton X-100 and then blocked with 5% BSA in PBS. To detect monocytes, cells were stained with anti-human CD14 monoclonal antibody (Abcam, UK, ab182032) overnight at 4°C. Endosomal markers early endosome antigen 1 (EEA1), lysosomal associated membrane protein 1 and 2 (LAMP1 and LAMP2) in monocytes were stained with anti-EEA1, anti-LAMP1, and anti-LAMP2 antibodies (Abcam, UK, ab109110, ab62562, ab18528) overnight at 4°C. The cells were washed with PBS and stained with Alexa Fluor 594 anti-mouse IgG (Invitrogen, USA, 2110496) for 1 h, and then mounted with mounting medium with DAPI (Santa Cruz, USA, 10319). The dishes were examined under an Olympus confocal microscope. Co-localization of EEA1 $^+$, LAMP1 $^+$, and LAMP2 $^+$ with the $A\beta_{42}$ immunoreactive area was quantified using ImageJ (NIH) as previously described [22].

$A\beta$ Degradation Assay

Isolated human monocytes were incubated with $A\beta_{42}$ overnight under the same conditions. After that, the medium containing $A\beta_{42}$ was thoroughly removed and stored at −80°C for ELISA testing. Monocytes were washed 3 times with PBS to remove extracellular $A\beta_{42}$ and re-seeded on 6-pore plates with 100 μg/mL PSK or the same volume of PBS. The monocytes were cultured for another 72 h, and then the cells were lysed with RIPA buffer (Beyotime, China, P0013B) for protein extraction. Extracellular and intracellular $A\beta_{42}$ levels were measured using ELISA kits (Invitrogen, USA, KHB3544). The results were normalized to total cellular protein.

Intraperitoneal Injection of PSK in Mice

APP/PS1 transgenic mice were obtained from Jackson Laboratory and bred in the Animal House of the Third Military Medical University. The husbandry procedures were approved by the Third Military Medical University Animal Welfare Committee.

PSK was dissolved in PBS at a stock concentration of 20 mg/mL and stored at −80 °C in aliquots of 100 μL. The frozen PSK was thawed immediately before use. Prior to initiation of $A\beta$ deposition, APP/PS1 transgenic mice aged 3 months were randomly assigned to be treated with PSK (2 mg/mouse, 3 times/week for 6 months, $n = 8$/group) or control PBS (3 times/week for 6 months, $n = 8$/group).

Behavioral Tests

Mice in the experiment underwent multiple behavioral tests – the Y-maze, open field, and Morris water maze – as previously described [23]. In brief, alternation was defined as successive entries into three arms on overlapping triplet sets. The percentage of alternation, defined as the total number of alternations $\times 100/$ (total number of arm entries -2), was calculated. In the open field test, each mouse was put in the center of the open field apparatus and left for 5 min. Rearing, grooming, defecation, urination, paths and distance travelled were recorded. The Morris water maze test consisted of three platform trials per day for 5 consecutive days, followed by a probe trial. The length of the path and escape latency were measured in platform trials. The annulus crossings and the time spent in each quadrant and were measured in probe trials. The novel arm exploration test was also conducted in a Y-maze.

After completion of the behavioral tests and blood collection, mice were humanely killed with an overdose of anesthetic and perfused transcardially with saline. One-hemisphere per animal was frozen or fixed in 4% paraformaldehyde for biochemical or histological analysis.

AD-type pathology and quantification

Coronal brain sections were cut at 30 μm and stored at 4°C in PBS containing 0.1% sodium azide. Five equally-spaced sections (~ 1.3 mm apart) were used for different types of staining. Compact Aβ plaques were stained using Congo red and total (both compact and diffuse) Aβ plaques were visualized using antibody 6E10 (Biolegend, USA, 803016) immuno-histochemistry as previously described [24, 25]. Immunofluorescence of NeuN and caspase-3 (Abcam, UK, ab104224 and ab13847) double staining was to detect apoptosis in neuronal cells. Immunofluorescence of NeuN and microtubule-associated protein (MAP)-2 (Abcam, UK, ab104224 and ab183830) double staining was used to assess neuronal loss and degeneration. Astrocytosis and microgliosis were visualized using immunohistochemistry of anti-glial fibrillary acidic protein (GFAP) and anti-CD68 antibodies (Abcam, UK, ab125212) to identify activated microglia, and anti-GFAP (Abcam, UK, ab134436) antibody to identify astrocytes. ImageJ software was applied to quantify the area fraction and/or density of positive staining and the number of cells. Immunofluorescence of double staining for Iba-1 (Wako, Japan, 019-19741) and 6E10 (Biolegend, USA, 803016) was conducted to verify the Aβ uptake by microglia. An Olympus confocal microscope was used to measure the co-localization of Iba1 and Aβ staining. The percentage of microglia co-localization with Aβ was quantified by an investigator who was blinded to group information using ImageJ.

ELISA Assays

Frozen brain was homogenized in liquid nitrogen, and part of the resultant powder was extracted 8successively with TBS, 2% (wt/vol) SDS, and 70% (vol/vol) formic acid (FA). The concentrations of Aβ40, Aβ42 (Invitrogen, USA, KHB3544 and KHB3481), IL-6, IL-1β, INF-γ, TNF-α (RayBio, USA, ELM-IL6, ELM-IL1b, ELM-IFNg, and ELM-TNFa) in brain extracts were measured by ELISA according to the manufacturer's instructions.

Western Blot

Western blot was used to analyze the levels of Aβ metabolism, phosphorylated Tau, and lysosomal Aβ-degrading enzymes. RIPA buffer was used for protein extraction from brain homogenates. The samples were loaded onto SDS-PAGE gels (4%–20% acrylamide) (Key-GEN, Nanjing, China). The separated proteins were transferred to nitrocellulose membranes. The blots were detected with the following antibodies: anti-APP C-terminal (Millipore, USA, 171610) to detect the C-terminal fragment (CTF)-α and CTF-β; anti-Aβ (BioLegend, USA, 803016) to detect Aβ and full-length APP (APPfl); anti-sAPP (Sigma, USA, 22C11) to detect secreted APP (sAPP)-α (sAPPα) or sAPPβ; anti-β-secretase (BACE)-1 (Abcam, UK, ab2077); anti-disintegrin and metalloprotease 10 (ADAM10) (Abcam, UK, ab1997); anti-presenlin 1 (PS1) (Cell signaling, USA, #5643); anti-insulin-degrading enzyme (IDE) (Abcam, UK, ab32216); anti-neprilysin (NEP) antibody (Millipore, USA, AB5458); anti-receptor for advanced glycation end products (Millipore, USA, MAB5328); anti-low density lipoprotein receptor-related protein 1 (LRP-1) (Abcam, UK, ab92544); anti-phosphorylated-Tau antibodies: anti-PS396 (Signalway, USA, 11102), anti-PS231 (Signalway, USA, 11110), anti-total tau (Millipore, USA, ab80579); and anti-β-actin (Sigma, USA, A1978). The membranes were incubated with IRDye 800 CW secondary antibodies (LiCOR, Lincoln, USA) and scanned by an Odyssey fluorescence scanner. The band density was normalized to β-actin for analysis.

Statistical Analysis

All data are presented as the mean ± SEM unless otherwise stated. Statistical comparisons between two groups were made using Student's *t* test or the Mann-Whitney U test, where appropriate. One-way ANOVA and Tukey's test were used to compare three groups. $P < 0.05$ (two-sided) were considered significant. All analyses were performed with GraphPad Prism software version 7.0, or SPSS software version 20.0.

Results

PSK Enhances Uptake and Degradation of $A\beta_{42}$ by Monocytes

To test whether PSK enhances $A\beta_{42}$ uptake by human monocytes, flow cytometry was used to quantify their internalization of $A\beta_{42}$. Side-scatter and forward-scatter, along with the biomarker of monocyte, CD14, were identified (Fig. 1A and B). Quantification of the mean fluorescence intensity (MFI) of FITC-positive $A\beta_{42}$ in monocytes showed that uptake of FITC-$A\beta_{42}$ by monocytes was enhanced, depending on PSK concentration (0–200 µg/mL, $P <0.001$), 100 µg/mL being the best PSK stimulating concentration (Fig. 1C–E). Further, we determined whether the degradation of internalized $A\beta_{42}$ by monocyte was influenced by PSK. Prior to treatments, monocytes were incubated with $A\beta_{42}$ overnight under the same conditions. We found no significant difference in extracellular $A\beta_{42}$ levels between groups, showing that there was no statistical difference in the uptake of $A\beta_{42}$ by untreated monocytes (Fig. 1F). After removal of extracellular $A\beta_{42}$, PSK (100 µg/mL) and PBS were randomly assigned to two groups and incubated for another 72 h. The

degradation of $A\beta_{42}$ by monocytes was significantly enhanced by PSK (Fig. 1G, $P <0.05$).

PSK Increases Expression of TLR2 and Intracellular Processing of $A\beta_{42}$ by Monocytes

Then, we used flow cytometry to characterize the influence of PSK on the ability of monocytes to recognize $A\beta$ associated with AD neuropathology. We tested the major surface receptors involved in the myeloid cell-mediated physiological uptake of $A\beta$: TLR2, TREM2, CD36, and SCARA1. We found that the expression of TLR2 was significantly enhanced by PSK, with no significant differences between groups in expression of the other surface receptors (Fig. 2A–I). To investigate whether the enhanced uptake of $A\beta$ by monocytes is directly mediated by increased expression of TLR2 activated by PSK, we used a TLR2 antagonist before adding PSK and found that the stimulating action of PSK was almost counteracted, with lower $A\beta_{42}$ uptake than by monocytes without the antagonist (Fig. 2J). In contrast to the PBS control, the co-localization of $A\beta_{42}$ with EEA1 and Lamp)1 and Lamp-2 within lysosomal vacuoles were more apparent in monocytes treated with PSK (Fig. 2K–M). Calculation of the
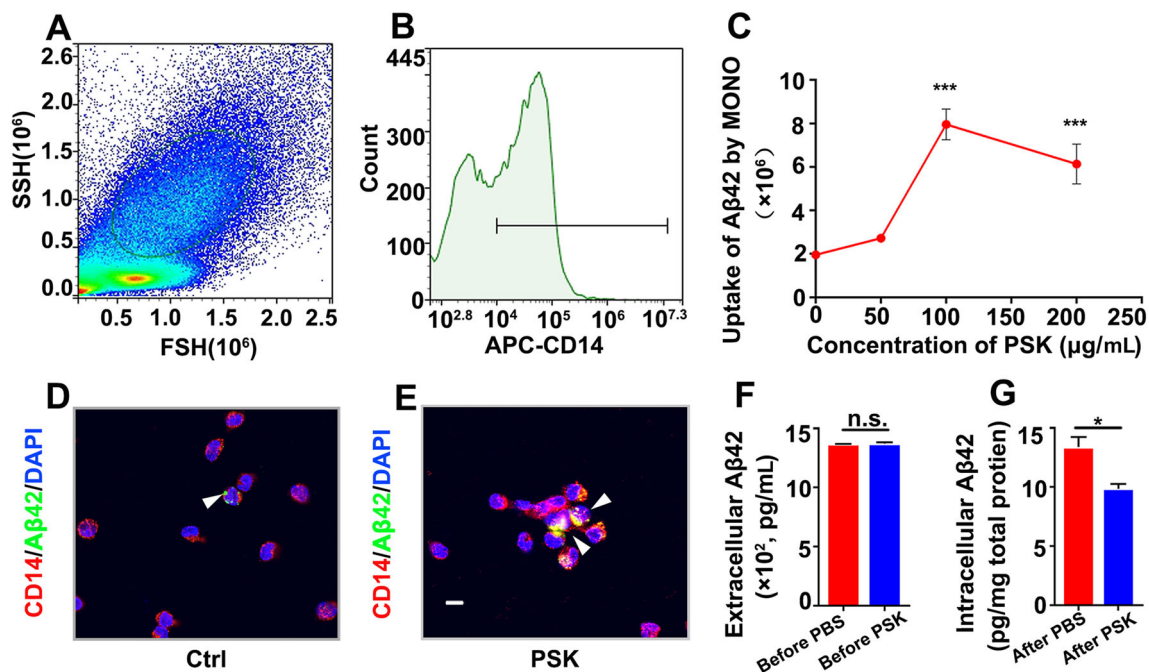
Fig. 1 PSK enhances uptake and degradation of $A\beta_{42}$ by monocytes in vitro. **A, B** Monocytes are selected by high-intensity CD14 labelling followed by gating of FSC-H and SSC-H. **C** $A\beta_{42}$ uptake by monocytes *versus* dose of PSK. **D, E** Confocal stack images of $A\beta_{42}$ uptake by human monocytes stained with Alexa594-conjugated anti-CD14 monoclonal antibody (red) and counter stained with DAPI (blue); FITC-conjugated $A\beta_{42}$ is shown in green (scale bar, 10 µm). **F,** **G** Extracellular and intracellular $A\beta_{42}$ levels before and after intervention assessed by ELISA (mean ± SEM. of triplicate wells in each treatment group). *$P <0.05$, ***$P <0.001$, n.s, not significantly different, one-way ANOVA and Student's *t*-test. FSC, forward scatter; SSC, sideward scatter; PSK, polysaccharide kestin; Ctrl, control.
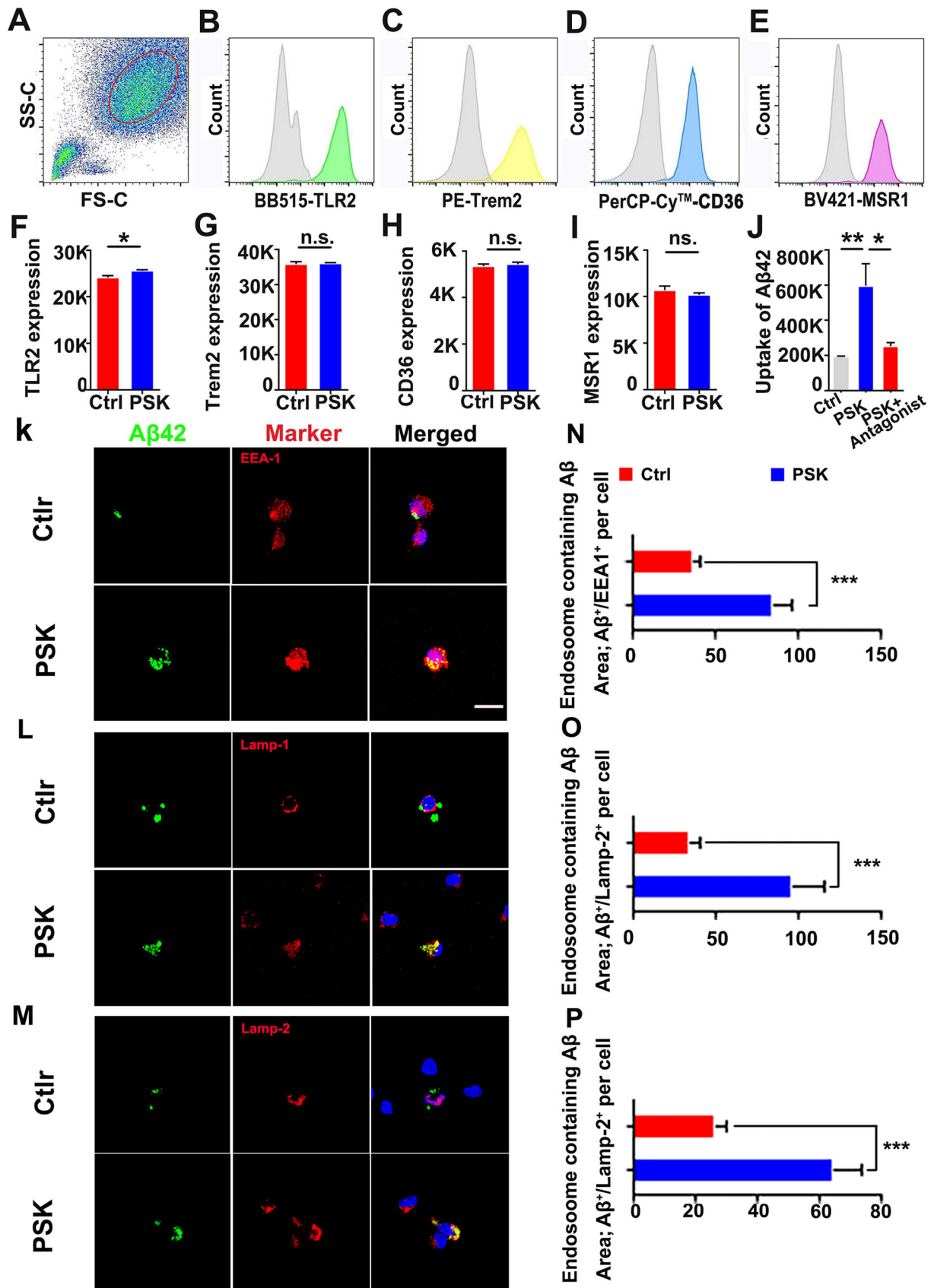
◄**Fig. 2** Detection of Aβ$_{42}$ uptake-related receptors and intracellular processing of Aβ$_{42}$ by monocytes treated with PSK in vitro. **A** Identification of monocytes by flow cytometry by FSC and SSC after CD14-positive selection by magnetic activated cell sorting. **B–E** Representative histograms showing the expression levels of TLR2, Trem2, CD36, and MSR1 in monocytes (grey curves indicate negative control staining). **F–I** Compared with controls, the expression level of TLR2 is increased in monocytes treated with PSK, with no significant difference between the two groups in the levels of TREM2, CD36, and MSR1. **J** Comparison of Aβ$_{42}$ uptake by monocytes between groups with different treatments. **K–M** Confocal stack images of PSK or PBS stimulated monocytes immunolabeled for FITC-Aβ$_{42}$ (green), endosomal markers (EEA1, Lamp-1, and Lamp-2, red), and nuclei (blue) (scale bar, 10 μm for all panels). **N–P** Immunoreactive areas of co-localized Aβ$_{42}$ and endosomal markers (EEA1, Lamp-1, and Lamp-2, red) in human monocytes in the two groups (mean ± SEM of triplicate wells in each treatment group). *P <0.05, **P <0.01, ***P <0.001, n.s, not significantly different, Student's t-test or one-way ANOVA. FSC, forward-scatter; SSC, side-scatter; PSK, polysaccharide kestin, Aβ, amyloid β-protein; TLR2, toll-like receptor 2; TREM2, triggering receptor expressed on myeloid cells 2; MSR1, macrophage scavenger receptor 1; EEA1, early endosome antigen 1; LAMP, lysosomal associated membrane protein.

Aβ$_{42}$ immunoactive area within EEA1$^+$, Lamp1$^+$, and Lamp2$^+$ revealed that monocytes treated with PSK had greater amounts of Aβ$_{42}$ in the endosomal-lysosomal pathway, contributing to more intracellular degradation (Fig. 2N–P). However, we did not find statistical differences between the PSK- and PBS-treated groups in the protein levels of the lysosomal Aβ-degrading enzymes cathepsin B, cathepsin D, and cathepsin S (Fig. S1).

PSK Improves Cognitive Deficits in APP/PS1 Mice

Based on its properties associated with the ability of monocytes to clear Aβ, we next investigated the preventive effects of PSK on AD-type pathology and cognitive deficits in APP/PS1 mice. All data *in vivo* presented below were from female AD mice. Compared with the PBS-treated APP/PS1 mice, the mice in the prevention (PSK-treated) group performed better in the Morris water maze, as reflected by a significant decrease in escape latency (Fig. 3A) in the successive platform learning trials, a greater number of annulus crossings (Fig. 3B), and more time spent in the target quadrant in the probe trial (Fig. 3C). In the novel arm exploration test, PSK-treated mice showed more entries into the novel arm than PBS-treated mice (Fig. 3D). In the spontaneous alteration test, the mice treated with PSK showed more total entries than PBS-treated mice (Fig. 3E). We also found a longer distance travelled in the PSK-treated group in the open filed test (Fig. 3F and G). These results indicate that PSK prevents the cognitive decline in APP/PS1 mice.
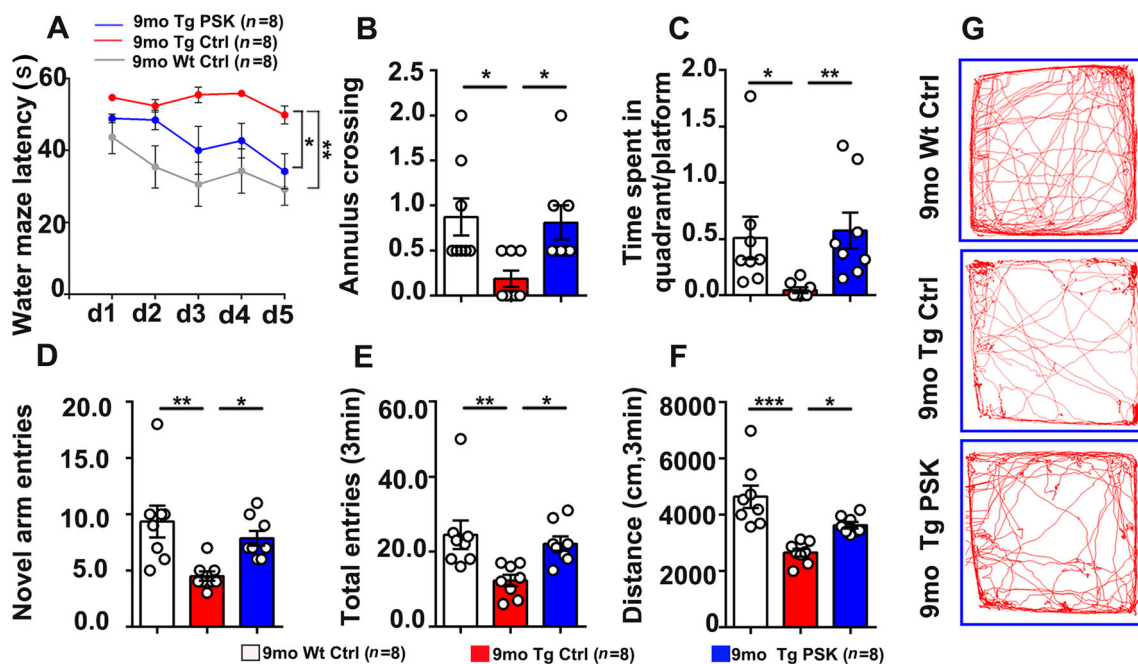
Fig. 3 PSK improves cognitive deficits in APP/PS1 mice. **A** Escape latency during platform trials in the Morris water maze. **B, C** Number of annulus crossings and time spent in the quadrant in probe test. **D, E** Number of novel entries and total entries in the Y-maze test. **F, G** Distance travelled and tracing graphs in the open field test. n = 8 per group, mean ± SEM, *P <0.05, **P <0.01, ***P <0.001, one-way ANOVA. Sec, second; PSK, polysaccharide kestin; Ctrl, control; WT, wild type mice; Tg, transgenic.

PSK Reduces Aβ Burden in APP/PS1 Mice

To investigate whether PSK affects the Aβ burden in APP/PS1 mice, Congo red staining and Aβ immunostaining (6E10) to detect compact and total amyloid plaques were performed, respectively. Compared with APP/PS1 controls, the mice treated with PSK had a significantly lower amyloid plaque burden in the brain (Fig. 4A–D). ELISA tests also showed a significant reduction in the levels of Aβ40 and total Aβ in the FA fraction and Aβ42 and total Aβ in the SDS fraction of brain homogenates, along with reduced serum Aβ42 in the PSK-treated group (Figs 4E–G and S2). Next, we investigated the potential mechanisms underlying the reduction of Aβ deposition after PSK treatment. Except for the Aβ level, there were no significant differences in the expression of APP and its metabolites, APPfl, sAPPα/β, CTF-β, and CTF-α (Fig. 4H–J). Moreover, there were no significant difference in the expression of enzymes associated with the Aβ-production and Aβ-degrading enzymes, ADAM10, BACE1 PS1, IDE, and NEP, between the two groups (Figs S3 and 4K, L). Interestingly, compared with control, the level of the Aβ transport receptor RAGE in homogenates was lower in PSK-treated mice (Fig. 4K and M), suggesting that PSK reduces the receptor-mediated influx of Aβ from the periphery into the brain through the blood-brain barrier (BBB). Next, we used flow cytometry to investigate the effects of PSK on Aβ42 uptake by monocytes in APP/PS1 mice *in vivo*. After morphological gating, the mouse monocytes were identified as CD45^{pos}/CD11b^{pos}/CD115^{pos} events and subsequently gated as Ly6C^{high} and Ly6C$^{low/neg}$ subsets (Fig. 5A–D). Although the Aβ42 uptake by the Ly6C$^{low/neg}$ subset was greater than that of the Ly6C^{high} subset, there was no significant difference in proportion of monocyte subsets between the PSK- and PBS-treated groups (Fig. 5E, F). Both TLR2 expression and Aβ42 uptake by mouse monocytes were greater in PSK-treated mice (Fig. 5G, H). By imaging flow cytometry, the internalized Aβ42 was more apparent in CD115-positive monocytes from PSK-treated mice than that of control (Fig. 5I–L). But we did not find significant differences in Aβ uptake by microglia and TLR2 expression in the AD mouse brain (Fig. S4).

PSK Rescues AD-related Pathology in the Brains of APP/PS1 Mice

Compared with PBS control, microgliosis (detected by CD68 antibody) and astrocytosis (detected by GFAP antibody) in the PSK-treated group were significantly decreased in the cortex (Fig. 6A–D). In addition, the levels of the pro-inflammatory cytokines TNF-α and IL-6 in brain homogenates in the treatment group were also lower than

Fig. 4 PSK reduces amyloid deposition in APP/PS1 mice. **A, B** ▶ Representative images of Congo red staining and statistics for fractional area of Congo red-positive plaques in the neocortex and hippocampus in APP/PS1 mice. Inset: representative morphology at a higher magnification. Scale bar, 1 mm. **C, D** 6E10 immunohistochemical staining (IHC) and 6E10-positive plaques in the neocortex (NC) and hippocampus (HC) in APP/PS1 mice. Inset: representative morphology at a higher magnification. Scale bar, 1 mm. **E–G** Aβ40, Aβ42 and Aβ40 + Aβ42 levels in TBS, 2% SDS, and 70% FA fractions of brain extracts in PSK-treated mice and controls assessed by ELISA. **H–J** Western blots and quantitative analysis of APP and its metabolites in brain homogenates. **K–M** Western blots and quantitative analysis of Aβ-degrading enzymes and Aβ-transporting receptors. $n = 8$ per group; mean ± SEM; *$P <0.05$, n.s, not significantly different, Student's *t*-test. PSK, polysaccharide kestin; Ctrl, control; WT, wild-type; Tg, transgenic; NC, neocortex; HC, hippocampus.

in PBS controls, with no significant difference in the levels of IFN-γ and IL-1β between groups (Fig. 6E–H). APP/PS1 mice treated with PSK showed markedly increased staining area fraction of NeuN (neurons) and MAP2 (dendrites), and decreased neuronal apoptosis (detected by caspase-3) in the hippocampus (Fig. 6I–N). Moreover, the area fractions of tau-phospho-Ser231-positive neurons in the neocortex of PSK-treated APP/PS1 mice were significantly lower than those of the controls, with no statistical difference in the area fractions of tau-phospho-Ser231-positive neurons in the hippocampus between the two groups (Fig. S5A, B). Western blots further showed that tau-phosphorylation at the serine 396 site was significantly lower in the brain of PSK-treated mice than controls, with no statistically significant difference in the expression of total tau (Tau5) between the two groups (Fig. S5C, D).

Discussion

Traditional anti-Aβ therapeutic strategies have primarily centered on clearing the brain Aβ. Recent studies have demonstrated that ∼40–60% of brain Aβ can diffuse into the blood and be cleared in the periphery, implying that the peripheral system also plays a pivotal role in clearing Aβ from the brain [4, 26, 27]. Despite emerging evidence demonstrating the critical role of peripheral Aβ clearance played by monocytes in AD [10, 28–30], our previous evidence showed that the ability of Aβ uptake by monocytes decrease with ageing and further decreases in AD patients, along with reduced expression of TLR2 [13]. TLR2 acts as a natural innate immune receptor for Aβ uptake, its malfunction impairs fibrillary Aβ42 uptake by human monocytes, and it delays cognitive decline in a mouse model of AD [20, 31]. Our current study found that PSK, an approved prescription for the treatment of multiple
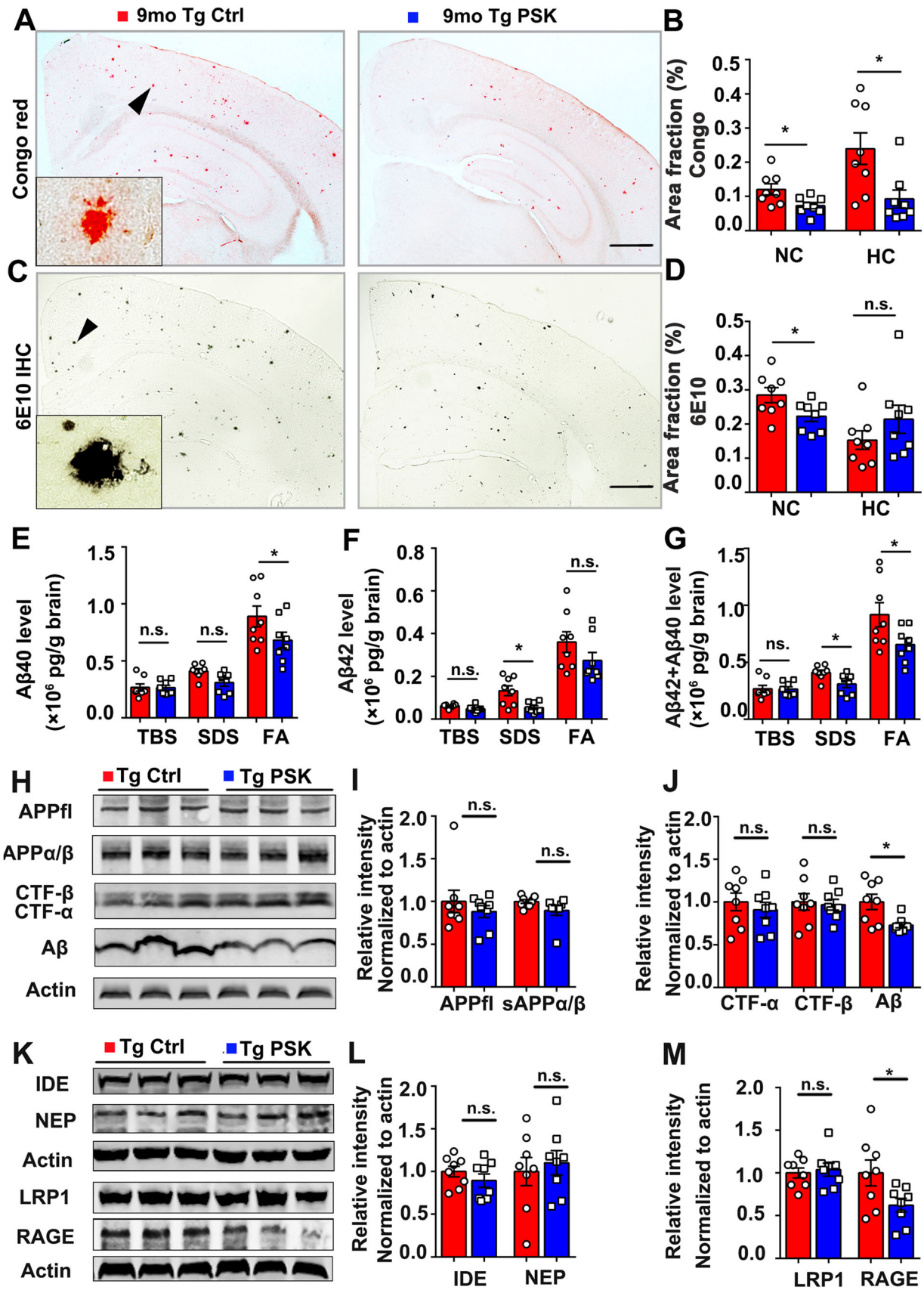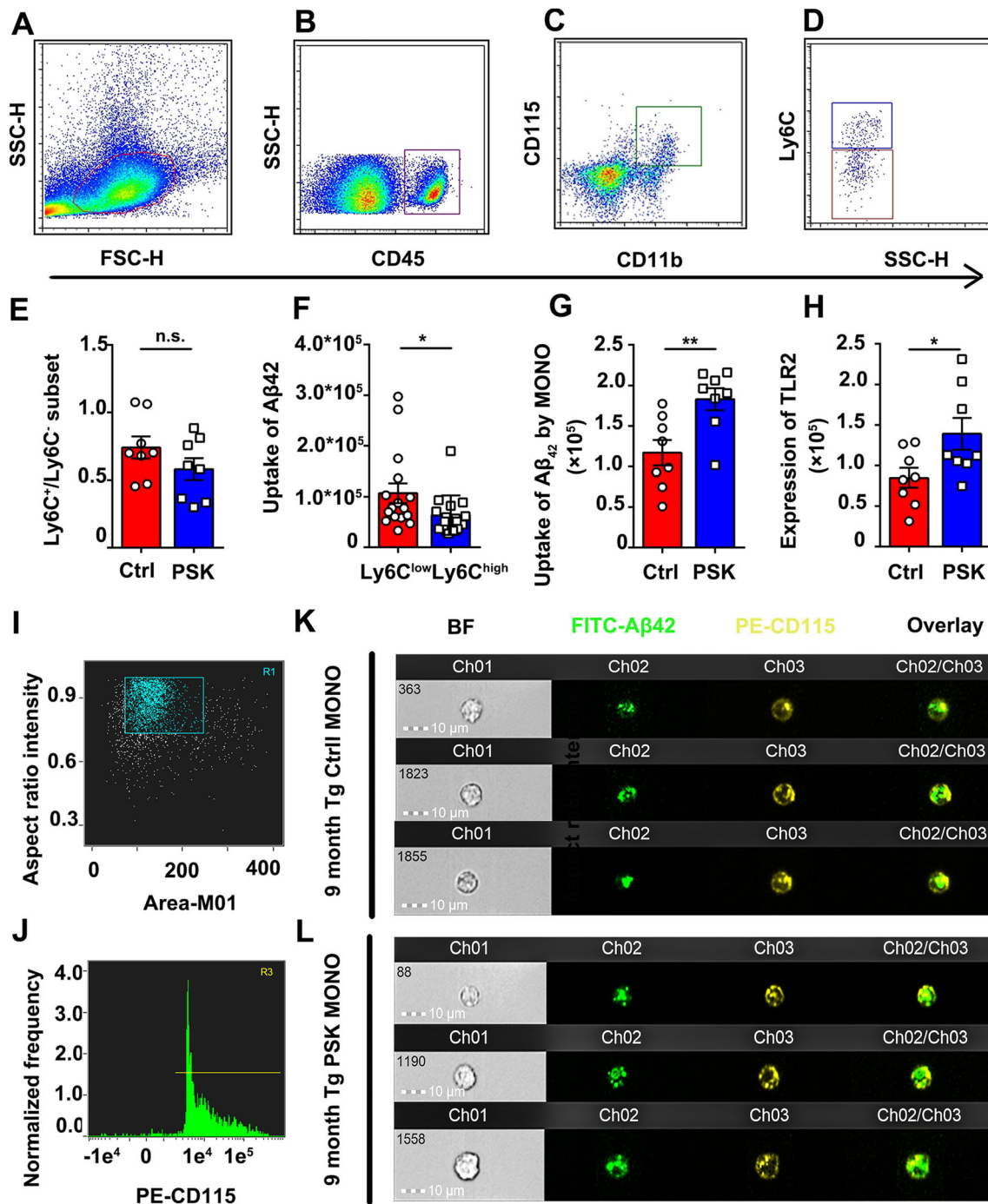
Fig. 5 Flow and imaging flow cytometry analysis of $A\beta_{42}$ uptake by mouse monocytes. **A, B** After morphological gating, mononuclear cells are selected as CD45-positive events. **C, D** Mouse monocytes are further identified as CD11b^pos/CD115^pos events and subsequently gated as Ly6C^high and Ly6C^low/neg subsets. **E, F** $A\beta_{42}$ uptake in monocyte subsets and effects of PSK on proportions of monocyte subsets, **G, H** $A\beta_{42}$ uptake and TLR2 expression in monocytes in control and PSK groups. **I, J** By imaging flow cytometry, cells with high-intensity CD115 labelling are selected as mouse monocytes, followed by selection of single cells gated on the area and aspect ratio of the bright-field image. **K, L** Images of FITC-labelled $A\beta_{42}$ uptake by mouse monocytes. $n = 8$ per group; mean ± SEM; $*P < 0.05$, $**P < 0.01$, n.s, not significantly different, Student's t-test. FSC, forward-scatter; SSC, side-scatter; PSK, polysaccharide kestin; Ctrl, control; WT, wild-type; Tg, transgenic; Aβ, amyloid-β.

cancers, not only stimulates TLR2-mediated uptake and intracellular metabolism of Aβ by monocytes, but also attenuates the cognitive impairment in an AD mouse model. These results indicate that PSK has the potential to intervene the pathogenesis of AD through enhancing the function of peripheral monocytes.
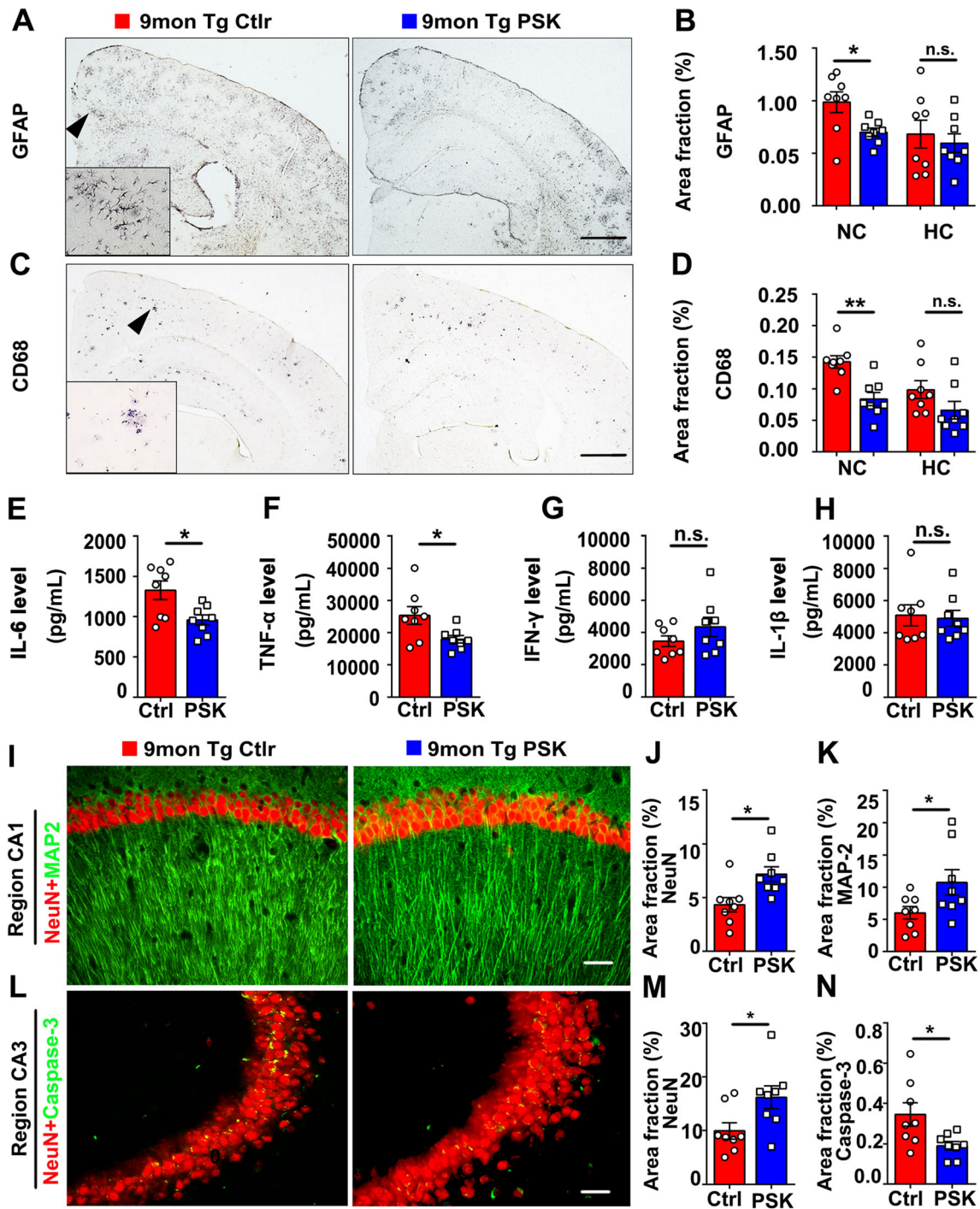
Fig. 6 PSK rescues inflammation and neuronal loss in the brains of APP/PS1 mice. **A–D** Immunostaining and quantification of activated astrocytosis (detected by GFAP) and microgliosis (detected by CD68). Insets: representative morphology at a higher magnification. Scale bars, 1 mm. (**E–H**) IL-6, TNF-α, IFN-γ, and IL-1β levels in brain homogenates from 9-month-old PSK-treated mice and controls. **I–K** MAP2 and NeuN immunostaining and quantification in the hippocampus and its subregions. Scale bar, 100 μm. **L–N** Neuronal apoptosis detected by activated caspase-3 (cas-3) immunofluorescence in CA3 of the hippocampus. Scale bar, 100 μm. $n = 8$ per group; mean ± SEM; *P <0.05, **P <0.01, n.s, not significantly different, Student's t-test. PSK, polysaccharide kestin; Ctrl, control; WT, wild-type; Tg, transgenic; NC, neocortex; HC, hippocampus.

In the present study, both the uptake and degradation of Aβ by monocytes were enhanced by PSK. Among the major surface receptors involved in the myeloid cell-mediated physiological uptake of Aβ [32], TLR2 expression was specifically increased with PSK, and this stimulatory action of PSK was almost counteracted by a TLR2

antagonist, suggesting that the enhanced Aβ uptake by monocytes induced by PSK may be mediated by the activation of TLR2. Besides, evaluation of the Aβ immunoreactive area revealed that PSK-treated monocytes had greater amounts of Aβ in the endosomal-lysosomal pathway, indicating greater intracellular Aβ processing, thus leading to more Aβ transport to lysosomes for degradation. Although we did not find any significant difference between the two groups in the molecular expression of Aβ degradative enzymes, we cannot rule out the possibility that cathepsin protease activity is enhanced by PSK.

It is noteworthy that the Aβ levels both in the brain and blood were significantly reduced by injection of PSK in APP/PS mice. We did not find any difference between the PSK treatment group and the control in the expression of APP and its metabolites, enzymes associated with Aβ production, and Aβ-degrading enzymes in the brain of AD mice, suggesting that PSK may not take part in the reduction of Aβ production or enhancement of Aβ degradation in the brain. The levels of Aβ influx transport receptors across the BBB (RAGE) were lower in PSK-treated mice than in controls, indicating that PSK reduces the influx of Aβ from the periphery into the brain through the BBB, allowing PSK-activated monocytes to play their role in peripheral Aβ clearance. Along with reduction of brain Aβ, we also found that PSK plays roles in neuroprotection and anti-inflammation, as reflected by increased numbers of neurons and down-regulation of neuronal apoptosis, dendritic spine shrinkage, microgliosis, and astrocytosis in response to Aβ. Another hallmark of AD is neurofibrillary tangles, which are caused by the hyperphosphorylation of tau protein and have been consistently correlated with cognitive function in patients [33–35]. In the current study, we found that PSK suppressed the hyperphosphorylation of tau in response to Aβ. These findings indicate that PSK suppresses downstream pathologies, including tau hyperphosphorylation, neuroinflammation, and neuronal loss.

However, neither the Aβ uptake by microglia nor the expression of TLR2 in the brain of AD mice were influenced by PSK, and the related mechanisms remain unclear. One possible explanation may be that with higher Aβ concentration and inflammation in the microenvironment of AD brain in which microglia reside, activation of TLR may have little effect on the already dysfunctional microglia. Another explanation may be that the amount of PSK that can enter the brain is limited, thus constraining the effect of PSK in the AD brain. These results indicate that PSK plays its role mainly by enhancing Aβ recognition and processing by monocytes in the periphery, leading to more soluble Aβ outflow and clearance in the periphery.

Conclusions

In summary, we suggest the potential application of PSK for the prevention of AD *via* Aβ clearance by peripheral monocytes. Because PSK is currently used to treat cancer and is safe in humans, the promising data from our current study warrant future clinical trials to test its therapeutic efficacy for AD.

References

1. Prince M, Bryce R, Albanese E, Wimo A, Ribeiro W, Ferri CP. The global prevalence of dementia: a systematic review and metaanalysis. Alzheimers Dement 2013, 9: 63–75.e62. https://doi.org/10.1016/j.jalz.2012.11.007.

2. Moschetti K, Cummings PL, Sorvillo F, Kuo T. Burden of Alzheimer's disease-related mortality in the United States, 1999–2008. J Am Geriatr Soc 2012, 60: 1509–1514.

3. Mawuenyega KG, Sigurdson W, Ovod V, Munsell L, Kasten T, Morris JC. Decreased clearance of CNS beta-amyloid in Alzheimer's disease. Science 2010, 330: 1774.

4. Xiang Y, Bu XL, Liu YH, Zhu C, Shen LL, Jiao SS, *et al*. Physiological amyloid-beta clearance in the periphery and its therapeutic potential for Alzheimer's disease. Acta Neuropathol 2015, 130: 487–499.

5. Yuede CM, Lee H, Restivo JL, Davis TA, Hettinger JC, Wallace CE, *et al*. Rapid *in vivo* measurement of β-amyloid reveals biphasic clearance kinetics in an Alzheimer's mouse model. J Exp Med 2016, 213: 677–685.

6. Qosa H, Abuasal BS, Romero IA, Weksler B, Couraud PO, Keller JN, *et al*. Differences in amyloid-β clearance across mouse and human blood-brain barrier models: Kinetic analysis and mechanistic modeling. Neuropharmacology 2014, 79: 668–678.

7. Butovsky O, Kunis G, Koronyo-Hamaoui M, Schwartz M. Selective ablation of bone marrow-derived dendritic cells increases amyloid plaques in a mouse Alzheimer's disease model. Eur J Neurosci 2007, 26: 413–416.

8. Koronyo-Hamaoui M, Ko MK, Koronyo Y, Azoulay D, Seksenyan A, Kunis G, *et al*. Attenuation of AD-like neuropathology by harnessing peripheral immune cells: Local elevation of IL-10 and MMP-9. J Neurochem 2009, 111: 1409–1424.

9. Koronyo Y, Salumbides BC, Sheyn J, Pelissier L, Li SL, Ljubimov V, *et al*. Therapeutic effects of glatiramer acetate and grafted CD115⁺ monocytes in a mouse model of Alzheimer's disease. Brain 2015, 138: 2399–2422.

10. Simard AR, Soulet D, Gowing G, Julien JP, Rivest S. Bone marrow-derived microglia play a critical role in restricting senile plaque formation in Alzheimer's disease. Neuron 2006, 49: 489–502.

11. Hui H, Fuller KA, Erber WN, Linden MD. Imaging flow cytometry in the assessment of leukocyte-platelet aggregates. Methods 2017, 112: 46–54.

12. Fiala M, Lin J, Ringman J, Kermani-Arab V, Tsao G, Patel A, *et al*. Ineffective phagocytosis of amyloid-beta by macrophages of Alzheimer's disease patients. J Alzheimers Dis 2005, 7:

302

Neurosci. Bull. March, 2022, 38(3):290–302

221–232; discussion 255–262. https://doi.org/10.3233/jad-2005-7304.

13. Chen SH, Tian DY, Shen YY, Cheng Y, Fan DY, Sun HL, et al. Amyloid-beta uptake by blood monocytes is reduced with ageing and Alzheimer's disease. Transl Psychiatry 2020, 10: 423.

14. Tahara K, Kim HD, Jin JJ, Maxwell JA, Li L, Fukuchi K. Role of toll-like receptor signalling in Abeta uptake and clearance. Brain 2006, 129: 3006–3019.

15. Reed-Geaghan EG, Savage JC, Hise AG, Landreth GE. CD14 and toll-like receptors 2 and 4 are required for fibrillar A{beta}-stimulated microglial activation. J Neurosci 2009, 29: 11982–11992.

16. Blander JM, Medzhitov R. Regulation of phagosome maturation by signals from toll-like receptors. Science 2004, 304: 1014–1018.

17. Kanazawa M, Mori Y, Yoshihara K, Iwadate M, Suzuki S, Endoh Y, et al. Effect of PSK on the maturation of dendritic cells derived from human peripheral blood monocytes. Immunol Lett 2004, 91: 229–238.

18. Maehara Y, Tsujitani S, Saeki H, Oki E, Yoshinaga K, Emi Y, et al. Biological mechanism and clinical effect of protein-bound polysaccharide K (KRESTIN(®)): Review of development and future perspectives. Surg Today 2012, 42: 8–28.

19. Lu HL, Yang Y, Gad E, Wenner CA, Chang A, Larson ER, et al. Polysaccharide krestin is a novel TLR2 agonist that mediates inhibition of tumor growth via stimulation of CD8 T cells and NK cells. Clin Cancer Res 2011, 17: 67–76.

20. Richard KL, Filali M, Préfontaine P, Rivest S. Toll-like receptor 2 Acts as a natural innate immune receptor to clear amyloid beta 1–42 and delay the cognitive decline in a mouse model of Alzheimer's disease. J Neurosci 2008, 28: 5784–5793.

21. Gambuzza ME, Sofo V, Salmeri FM, Soraci L, Marino S, Bramanti P. Toll-like receptors in Alzheimer's disease: A therapeutic perspective. CNS Neurol Disord Drug Targets 2014, 13: 1542–1558.

22. Koronyo-Hamaoui M, Sheyn J, Hayden EY, Li SL, Fuchs DT, Regis GC, et al. Peripherally derived angiotensin converting enzyme-enhanced macrophages alleviate Alzheimer-related disease. Brain 2020, 143: 336–358.

23. Jiao SS, Yao XQ, Liu YH, Wang QH, Zeng F, Lu JJ, et al. Edaravone alleviates Alzheimer's disease-type pathologies and cognitive deficits. Proc Natl Acad Sci USA 2015, 112: 5225–5230.

24. Yao XQ, Jiao SS, Saadipour K, Zeng F, Wang QH, Zhu C, et al. p75NTR ectodomain is a physiological neuroprotective molecule against amyloid-beta toxicity in the brain of Alzheimer's disease. Mol Psychiatry 2015, 20: 1301–1310.

25. Xiong HQ, Callaghan D, Wodzinska J, Xu JJ, Premyslova M, Liu QY, et al. Biochemical and behavioral characterization of the double transgenic mouse model (APPswe/PS1dE9) of Alzheimer's disease. Neurosci Bull 2011, 27: 221–232.

26. Wang J, Gu BJ, Masters CL, Wang YJ. A systemic view of Alzheimer disease - insights from amyloid-β metabolism beyond the brain. Nat Rev Neurol 2017, 13: 703.

27. Liu YH, Wang YR, Xiang Y, Zhou HD, Giunta B, Mañucat-Tan NB, et al. Clearance of amyloid-beta in Alzheimer's disease: Shifting the action site from center to periphery. Mol Neurobiol 2015, 51: 1–7.

28. El Khoury J, Toft M, Hickman SE, Means TK, Terada K, Geula C, et al. Ccr2 deficiency impairs microglial accumulation and accelerates progression of Alzheimer-like disease. Nat Med 2007, 13: 432–438.

29. Thériault P, ElAli A, Rivest S. The dynamics of monocytes and microglia in Alzheimer's disease. Alzheimers Res Ther 2015, 7: 41.

30. Feng Yu, Lei Li, Xiaohong Sun. Monocytes and Alzheimer's disease. Neurosci Bull 2011, 27: 115–122.

31. Udan ML, Ajit D, Crouse NR, Nichols MR. Toll-like receptors 2 and 4 mediate Abeta(1–42) activation of the innate immune response in a human monocytic cell line. J Neurochem 2008, 104: 524–533.

32. Zuroff L, Daley D, Black KL, Koronyo-Hamaoui M. Clearance of cerebral Aβ in Alzheimer's disease: Reassessing the role of microglia and monocytes. Cell Mol Life Sci 2017, 74: 2167–2201.

33. Gordon BA, Blazey TM, Su Y, Hari-Raj A, Dincer A, Flores S, et al. Spatial patterns of neuroimaging biomarker change in individuals from families with autosomal dominant Alzheimer's disease: A longitudinal study. Lancet Neurol 2018, 17: 241–250.

34. Han SD, Gruhl J, Beckett L, Dodge HH, Stricker NH, Farias S, et al. Beta amyloid, tau, neuroimaging, and cognition: Sequence modeling of biomarkers for Alzheimer's Disease. Brain Imaging Behav 2012, 6: 610–620.

35. Lantero Rodriguez J, Karikari TK, Suárez-Calvet M, Troakes C, King A, Emersic A, et al. Plasma p-tau181 accurately predicts Alzheimer's disease pathology at least 8 years prior to post-mortem and improves the clinical characterisation of cognitive decline. Acta Neuropathol 2020, 140: 267–278.